Noise sensitivity analysis of a two-stage baseplate fastening system

Evangelos Ntotsios[1], Boniface Hima[1], David Thompson[1], Giacomo Squicciarini[1] and David Herron[2]

[1] Institute of Sound and Vibration Research, University of Southampton, Southampton SO17 1BJ, United Kingdom
[2] Pandrol, 63 Station Road, Addlestone, Surrey KT15 2AR, United Kingdom
e.ntotsios@soton.ac.uk

Abstract. A study is presented into the sensitivity of rolling noise to design changes in a two-stage baseplate rail fastening system. The focus is on the influence on the rolling noise of three parameters of the fastening system: the stiffnesses of the railpad and the baseplate pad and the thickness of the baseplate that determines its mass and sound radiation ratio. The TWINS model is adapted by introducing the baseplate vibration and sound radiation using results from an experimentally verified 2.5D finite element model. Based on the simulations, an optimum railpad stiffness is identified of around 500 MN/m, based on a baseplate pad stiffness value of 80 MN/m. The thickness of the baseplate has only a small effect on the total rolling noise.

Keywords: Rolling Noise, Baseplate Rail Fastener, Sound Radiation.

1 Introduction

There are several commercially available two-stage baseplate designs, each of which consists of a metal baseplate between two elastic pads: the railpad, which is usually stiffer, and the baseplate pad, which is softer and is placed under the baseplate. To minimize vibration transmission to the foundation and the ground the overall stiffness should be kept as low as possible. This is mainly governed by the stiffness of the lower pad. On the other hand, the stiffness of the railpad and the mass of the baseplate affect the track decay rates (TDRs) and thereby the rail component of rolling noise. Moreover, the flexural modes of vibration of the baseplate and the size of the radiating surface affect the sound radiation efficiency and thereby the baseplate radiated noise.

The overall rolling noise can be calculated as a combination of the noise radiated by the train wheels, the rails and the vibrating components of the track; for the case of a slab track with a two-stage fastening system these are the baseplates and the slab. The design of the fastening system will influence the wheel radiated noise only at low frequencies (i.e. below 1 kHz) and not at higher frequencies where the wheel contribution to the overall noise is significant [1]. Moreover, as the baseplate pad usually

has a low stiffness, the sound radiation from the slab will be negligible. Thus, the influence of the two-stage fastening design is important principally for the noise radiation from the rail and the baseplates.

The aim of this work is to quantify the influence on the rolling noise of three design parameters of the two-stage fastening system: the stiffnesses of the baseplate pad and the railpad and the thickness of the baseplate. For this, a computational strategy is used that represents the track using an experimentally validated 2.5D finite element (FE) model including the flexural response and radiation efficiency of the baseplates. These results are then used in combination with the TWINS model [2] to calculate the wheel-rail interaction forces and the wheel, rail and baseplate vibration and noise. The results can be used to identify baseplate fastening designs that minimise the noise.

2 Methodology

Separate numerical models are used for the rail and baseplate vibration in the frequency domain. The free infinite rail is represented by a 2.5D FE model whereas the metal baseplates and the lower pad are represented by a 3D FE model in Comsol. This is used to obtain a mobility matrix corresponding to nine positions beneath the rail pad (in a 3×3 arrangement). The rail is coupled to a large number of these baseplates, through discrete springs representing the railpads, using the method from [3]. The coupled track model is used to predict the rail mobilities and TDRs, and also the interaction forces between the railpads and the baseplates. These railpad forces are then introduced in the FE model of the baseplate to determine the velocities (due to a unit point load on the rail) at the FE nodes of the baseplate. The radiation ratio and radiated power of the multiple baseplates is calculated by applying the Rayleigh integral method to the predicted velocities of the baseplates.

The predicted rail point mobilities and TDRs from the coupled model are introduced into TWINS to calculate the wheel-rail interaction forces and the wheel and rail vibration and noise considering the wheel/rail roughness. On the other hand, the baseplate noise is determined by combining the wheel-rail forces with the results from the numerical track model. The overall track rolling noise due to the train passage is quantified as the sum of the sound power radiated by the rails and the baseplates for a 20 m section of the track.

3 Comparison with measured results

3.1 Model parameters

The two-stage baseplate design considered in this work consists of a cast-iron baseplate with a railpad above it and baseplate pad beneath it (Fig. 1(a)). The detailed baseplate geometry can be seen in Fig. 1(b). The baseplate has length 0.404 m and width 0.206 m, and it has a mass of 6.3 kg. The thickness of the plate body is 15 mm. Fig. 1(c) shows the FE model from which it can be seen that some of the detail of the clipping area was omitted; nevertheless, the vibration modes, in the frequency range

of interest, were validated against measurements on a free baseplate. The baseplate pad is represented by a layer of springs with hysteretic damping. From comparison with experiments, the vertical and lateral stiffness and damping loss factor were set to 80 MN/m and 60 MN/m and 0.12 respectively.

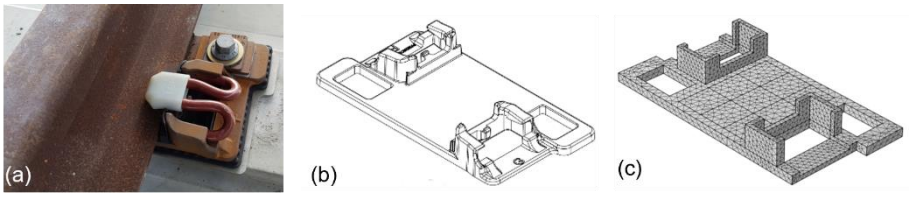

Fig. 1. Two-stage baseplate rail fastening system. (a) At the test track; (b) baseplate geometry; (c) baseplate 3D FE model.

In the track model, the rail is UIC60 and is discretely supported by 121 rail fasteners with 0.65 m spacing. The vertical stiffness used for the railpads was obtained from measurements for a selection of railpads [4]. The lateral railpad stiffness is assumed as 25% of the value used for the vertical stiffness.

3.2 Mobility measurements at the test track

Measurements of rail and baseplate mobility were made on a non-operational slab track located at the National College for Advanced Transport and Infrastructure at Doncaster, UK. The tests were performed on a 20 m section of track fitted with UIC60 rail on Pandrol two-stage rail fasteners for a selection of railpads with different stiffness. The measured rail and baseplate mobilities were then compared with the predictions from the numerical model using railpad stiffnesses obtained from [4].

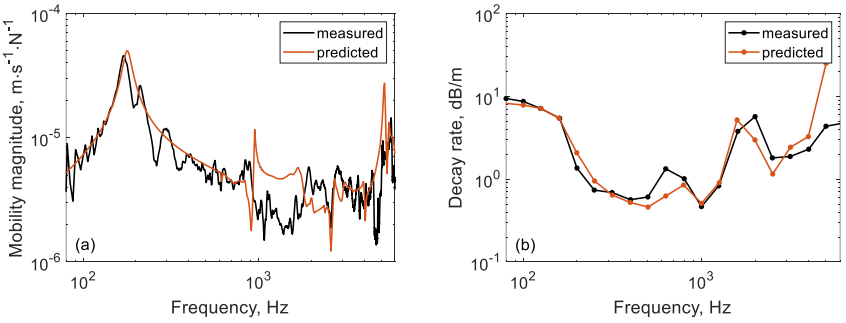

Fig. 2. Comparison between rail measurements and predictions from the numerical model. (a) Rail driving point mobility magnitude and (b) one-third octave TDR.

Fig. 2 compares the measured and predicted rail vertical responses for the case of a railpad with 310 MN/m vertical stiffness. A good agreement can be seen for both the driving point mobility and the TDR. The oscillations seen in the measured mobility

are due to reflections from the end of the finite rail of the test track. Similar good agreement was found for the other railpads tested (not shown).

3.3 Baseplate sound radiation measurements

A 6 m section of half-width slab track fitted with 8 two-stage baseplates (Fig. 3(a)) was installed in the reverberation chamber (Fig. 3(b)). The track was fitted with a 6 m UIC60 rail using railpads with 310 MN/m vertical stiffness and baseplate pads similar to the ones installed on the test track at Doncaster. Noise and vibration tests were conducted to validate the predictions from the numerical model.

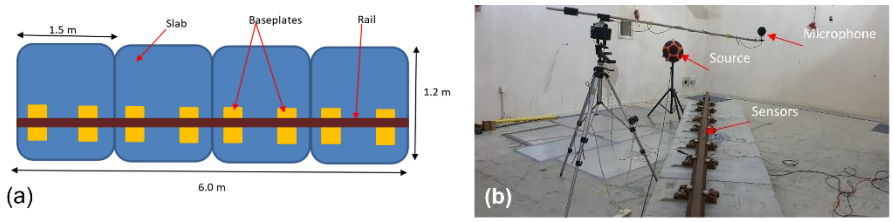

Fig. 3. Slab track test section. (a) Dimensions; (b) In the reverberation chamber.

To determine the radiation ratio σ, spatially-averaged mobilities were measured by impact hammer tests, and a reciprocity method was used to determine the sound power for a unit force [5]. The structure is excited by acoustic excitation from a known sound source and the resulting vibration of the structure is measured (Fig 3(b)).

Fig. 4(a) shows the measured and predicted baseplate vibration response. These results are for a single baseplate without the presence of the rail. A good agreement is found in the frequency range below 1 kHz. Above 1 kHz, there are differences between the frequencies of measured and predicted vibration modes, probably due to the geometric simplifications used for the 3D FE model; however, the general trend of the predicted velocities agrees with the measured one.

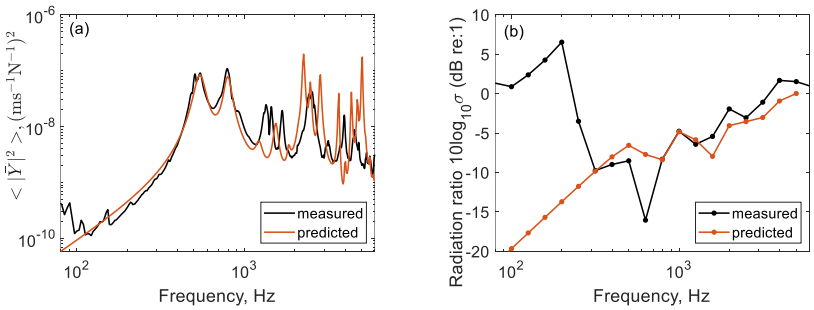

Fig. 4. Comparison between baseplate measurements and predictions. (a) Spatially averaged mean-squared mobility and (b) one-third octave radiation index ($10\log_{10}\sigma$).

The radiation ratio is shown in Fig. 4(b). The predicted results are calculated using the Rayleigh integral method with the predicted surface-averaged squared velocity from Fig. 4(a). The measured results below 300 Hz are believed to be affected by the radiation contribution of the slab (which had a thickness of only 0.2 m) and possibly the room floor, which are not included in the numerical model. A good agreement can be seen between the measured and the predicted results for frequencies above 300 Hz.

With the rail fitted on the slab track, the spatially averaged mobility of the rail and the baseplates were measured for excitation on the rail above the fourth baseplate. Fig. 5(a) shows the ratio of the squared vibration of the baseplates to that of the rail. A good agreement is obtained between 160 Hz and 2500 Hz. For frequencies outside this range, the measured values are higher than the predicted ones; the reason for these differences is unknown although simplifications in the model of the baseplate and the railpad may play a role.

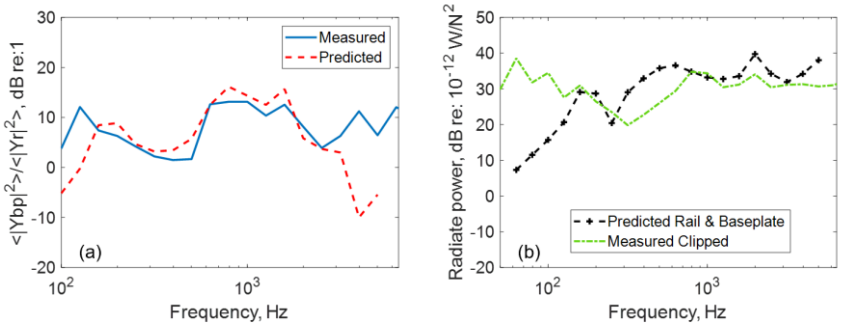

Fig. 5. Comparison between rail and baseplate measurements and predictions. (a) Spatially averaged transmissibility of the baseplates relative to the rail and (b) sound power due to a unit force on the railhead.

Fig. 5(b) shows the sound power from the track for a unit force. In the predictions, it is assumed that the radiated sound power from the rail and the baseplates can be treated as uncorrelated. The rail radiation is determined from the spatially averaged vibration calculated using the numerical track model combined with the radiation ratio from [6]. The baseplate sound radiation is calculated by using the radiation ratio calculated from the Rayleigh integral for 8 baseplates excited by the rail. The measured and predicted results show good agreement above 800 Hz. Between 315 Hz and 630 Hz, the measured sound power levels are lower than the predicted ones, but the difference is less than 10 dB. These differences are probably due to modelling and parametric uncertainty that affect the predicted results.

4 Noise sensitivity analysis

To investigate the effect of the baseplate design parameters, the radiated sound power during a train passage was calculated by using the proposed approach. Results were obtained for different values of baseplate pad stiffness, railpad stiffness and baseplate

thickness. For the TWINS calculations, the wheel is from a modern multiple unit train, with a diameter of 0.84 m and a straight web. The train speed is 120 km/h and measured rail roughness data used is from a typical ballasted track.

Figs. 6, 7 and 8 show the predicted TDRs, and total track sound power, i.e. from the rail and baseplates. The wheel noise is not shown but is around 103.4 dBA in all cases. Fig. 6 compares the predictions for different values of the baseplate pad stiffness (given in the legend) and a constant railpad stiffness of 310 MN/m. When increasing the baseplate pad stiffness, the TDR is increased at frequencies below 500 Hz, but is less affected at higher frequencies. Below 500 Hz the baseplate radiation efficiency, not shown here, decreases when the lower pad stiffness is increased. These differences in the TDRs and the baseplate radiation ratio affect the track radiated power, shown in Fig. 6(b), at frequencies below 500 Hz. A smaller influence (less than 4 dB) can be seen in the frequency range 500-1600 Hz. Nevertheless, the overall A-weighted sound power remains almost unaffected, with differences of less than 1.5 dB.

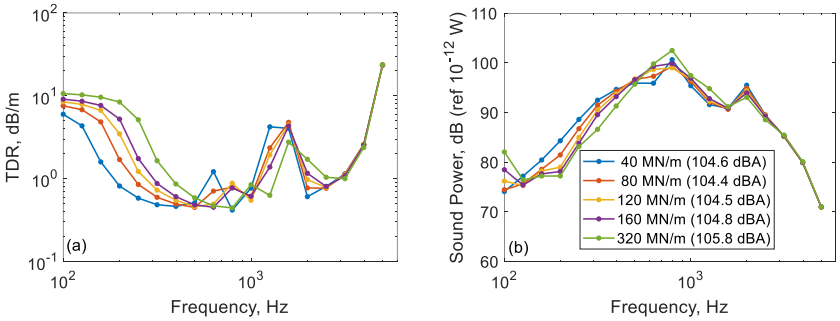

Fig. 6. One third octave comparison between predictions for different baseplate pad stiffness. (a) TDR and (b) track radiated sound power (unweighted).

In Fig. 7, the railpad stiffness is varied, while the baseplate pad stiffness is kept constant at 80 MN/m. When the railpad stiffness is increased, the TDR in Fig. 7(a) is increased at frequencies below 500 Hz and at higher frequencies, above 1.25 kHz. This reduces the average rail vibration and thus the radiated track sound power; however, above 1 kHz the baseplate vibration (not shown) is increased with stiffer railpads. For the highest values of railpad stiffness, the baseplate vibration becomes significant and its sound radiation in the frequency range 1.6 – 2.5 kHz dominates the track radiated sound, as can be seen by the higher levels in Fig. 7(b). Therefore, the overall A-weighted track sound power has a minimum for a railpad stiffness of 528 MN/m, for which it is about 4 dB lower than for the softest pad and 1 dB lower than for the stiffest one.

Finally, in Fig. 8, results are given for different thicknesses of the baseplate; these are for a baseplate pad stiffness of 80 MN/m and railpad of 310 MN/m. Below 1.25 kHz the TDR increases when the baseplate thickness (and hence mass) is increased; above 1.6 kHz, the effect on the TDR is reversed. However, over much of the fre-

quency range the radiation ratio of the baseplates (not shown) increases as the thickness is increased, by up to 4 dB below 1 kHz for this range of parameters. Consequently, at low frequencies, below 500 Hz, there is little change in the track radiated power in Fig. 8(b). Between 500 and 1250 Hz, the track sound power is reduced as the thickness is increased. The largest level difference between the thinnest and thickest baseplate is about 6 dB, which occurs at 800 Hz where the sound power has its maximum. In the frequency range 1.25 – 3.15 kHz, the increase of the baseplate thickness leads to an increase in the track sound power. However, the overall A-weighted track sound power level remains almost unchanged, with differences of less than 2 dB between the lowest and highest predicted values.

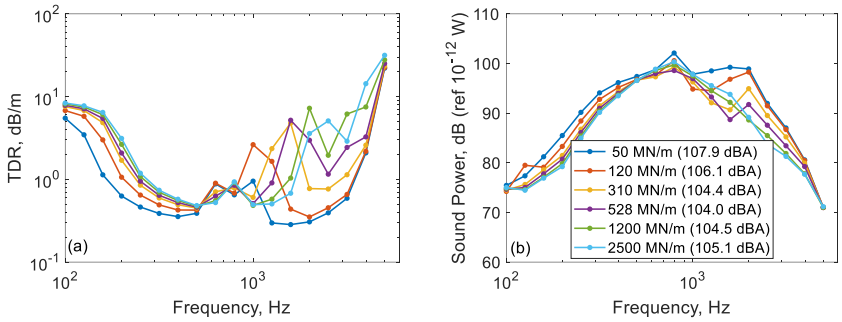

Fig. 7. One third octave comparison between predictions for different railpad stiffness. (a) TDR and (b) track radiated sound power (unweighted).

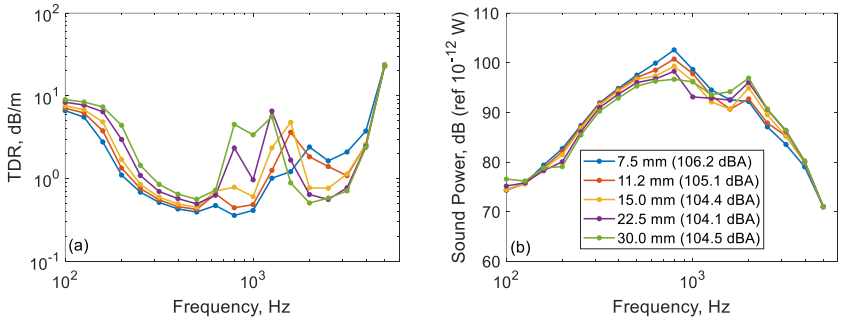

Fig. 8. One third octave comparison between predictions for different baseplate thickness. (a) TDR and (b) track radiated sound power (unweighted).

5 Conclusion

The effect of the various parameters of a two-stage baseplate on the rolling noise has been explored. It is concluded that the thickness (and mass) of the baseplate has only a small effect on the overall noise which would not justify the increase in material and cost of a heavier baseplate. The stiffness of the baseplate pad has only a small effect

on the total rolling noise from the track; however, a low stiffness is important to control the vibration transmission to the foundation and the ground. The railpad stiffness has the greatest effect on the noise, with variations in the track noise level of up to 4 dB. A stiff railpad can help to control the noise from the rail by increasing the TDR, but this occurs at the expense of increased noise from the baseplate itself. An optimum railpad stiffness is identified of around 500 MN/m, based on a baseplate pad stiffness value of 80 MN/m.

Acknowledgements

The authors gratefully acknowledge Pandrol for providing the rail-fastening system, railpads and organizing the measurement at the test track. The work described here has been supported by the EPSRC under the programme grant EP/M025276/1, 'The science and analytical tools to design long life, low noise railway track systems (Track to the Future)'.

References

1. Thompson, D.: Railway Noise and Vibration Mechanisms, Modelling and Means of Control. Elsevier, Oxford (2009).
2. Thompson, D., Hemsworth, B., Vincent, N.: Experimental validation of the TWINS prediction program for rolling noise, part 1: description of the model and method. Journal of Sound and Vibration 193(1), 123–135 (1996).
3. Zhang, X., Thompson, D., Li, Q., Kostovasilis, D., Toward, M., Squicciarini, G., Ryue, J: A model of a discretely supported railway track based on a 2.5 D finite element approach. Journal of Sound and Vibration 438, 153–174 (2019).
4. Hima, B., Thompson, D., Squicciarini, G., Ntotsios, E., Herron D.: Estimation of track decay rates and noise based on laboratory measurements on a baseplate fastening system. In: G. Degrande et al., editors, Noise and Vibration Mitigation for Rail Transportation Systems. Proceedings of the 13th International Workshop on Railway Noise, Ghent, Belgium, September 2019. Notes on Numerical Fluid Mechanics and Multidisciplinary Design 150 (2021) 621-628, Springer Nature Switzerland.
5. Squicciarini, G., Putra, A., Thompson, D., Zhang, X., Salim, M.A.: Use of a reciprocity technique to measure the radiation efficiency of a vibrating structure. Applied Acoustics 89, 107–121 (2015).
6. Zhang, X., Thompson, D., Quaranta, E., Squicciarini, G.: An engineering model for the prediction of the sound radiation from a railway track. Journal of Sound and Vibration 461, 114921 (2019).